NANO LETTERS
Cite This: Nano Lett. 2020, 20, 339−344
Letter
pubs.acs.org/NanoLett

Yu−Shiba−Rusinov States in the Charge-Density Modulated Superconductor $NbSe_2$

Eva Liebhaber,[†] Sergio Acero González,[‡] Rojhat Baba,[†] Gaël Reecht,[†] Benjamin W. Heinrich,[†] Sebastian Rohlf,[§] Kai Rossnagel,[§,∥] Felix von Oppen,[‡] and Katharina J. Franke*[,†]

[†]Fachbereich Physik and [‡]Dahlem Center for Complex Quantum Systems and Fachbereich Physik, Freie Universität Berlin, 14195 Berlin, Germany

[§]Ruprecht-Haensel-Labor and Institut für Experimentelle und Angewandte Physik, Christian-Albrechts-Universität zu Kiel, 24098 Kiel, Germany

[∥]Deutsches Elektronen-Synchrotron DESY, 22607 Hamburg, Germany

Supporting Information

ABSTRACT: $NbSe_2$ is a remarkable superconductor in which charge-density order coexists with pairing correlations at low temperatures. Here, we study the interplay of magnetic adatoms and their Yu−Shiba−Rusinov (YSR) bound states with the charge density order. Exploiting the incommensurate nature of the charge-density wave (CDW), our measurements provide a thorough picture of how the CDW affects both the energies and the wave functions of the YSR states. Key features of the dependence of the YSR states on adsorption site relative to the CDW are explained by model calculations. Several properties make $NbSe_2$ a promising substrate for realizing topological nanostructures. Our results will be important in designing such systems.

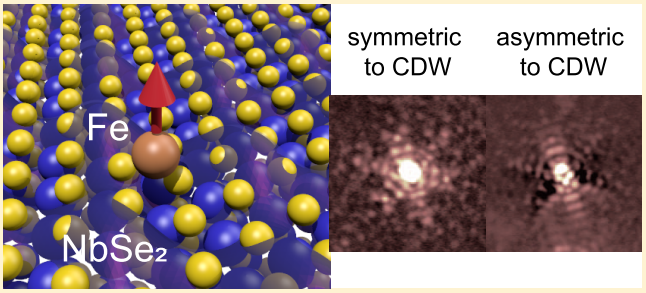

KEYWORDS: *Yu−Shiba−Rusinov states, superconductor, charge-density wave, $NbSe_2$, scanning tunneling spectroscopy*

$NbSe_2$ is a fascinating and in part still enigmatic superconductor. There is evidence for an anisotropic gap as well as multiband superconductivity[1−9] and the spin physics is highly nontrivial due to strong spin−orbit coupling, most prominently in monolayers of $NbSe_2$.[10,11] Already far above the superconducting transition, $NbSe_2$ undergoes a transition into a charge-density-wave (CDW) ordered state ($T_{CDW} \approx 33$ K) which coexists with superconductivity ($T_c \approx 7.2$ K) at low temperatures.[12−23] The precise interplay between CDW ordering and superconductivity remains only partially understood at present.[14,24−26]

At the same time, recent experiments suggest that $NbSe_2$ has attractive properties in the context of engineering topological superconducting phases.[27,28] Following the seminal work of Nadj-Perge et al.,[29] a topological phase and Majorana bound states can appear in chains of magnetic adatoms on superconducting substrates. One way to understand these remarkable phases is based on coupling Yu−Shiba−Rusinov (YSR) bound states[30,31] in the superconducting gap which are induced by individual adatoms.[32−35] Because of its layered structure, YSR states in $NbSe_2$ fall off laterally much more slowly than in three-dimensional superconductors.[36] This enhances the coupling between the YSR states of neighboring magnetic impurities,[37] potentially increasing the energy scale and thus the stability of possible topological phases. $NbSe_2$ is also a relatively robust material which may enable one to build nontrivial adatom structures from the bottom up by manipulation using a scanning tunneling microscope tip.

The YSR states of different adatoms hybridize particularly strongly when the YSR energies of the isolated adatoms are identical and their wave functions extend sufficiently far along their connecting line.[37−41] For $NbSe_2$, this is nontrivial to achieve due to the CDW ordering. Indeed, the CDW is incommensurate with the underlying atomic lattice so that adatoms, which are nominally identical in terms of their atomic adsorption site, will in general be positioned differently with respect to the CDW. Here, we observe that both the energy and the wave function of YSR states depend sensitively on the adatom position relative to the CDW and provide model calculations to understand these effects qualitatively. The dependence on the CDW imposes requirements which are crucial to take into account when designing adatom structures to realize topological superconducting phases.

To isolate the effect of the CDW on the YSR states, we focus on adatoms on clean 2*H*-$NbSe_2$ surfaces instead of buried impurities as used in previous experiments.[36,42] This gives us full control over the adsorption site and allows us to compare adatoms which differ only in their locations relative to the

Received: September 27, 2019
Revised: December 7, 2019
Published: December 16, 2019

DOI: 10.1021/acs.nanolett.9b03988
Nano Lett. 2020, 20, 339−344

CDW. Indeed, numerous previous studies[35,40,43−47] on other substrates have shown that in the absence of CDW ordering, YSR spectra and wave functions are fully reproducible for a particular adsorption configuration of the adatom on the substrate.

A clean 2*H*-$NbSe_2$ surface is prepared by cleaving a bulk crystal (grown by iodine vapor transport[16]) in ultrahigh vacuum. Scanning tunneling spectroscopy (performed by standard lock-in techniques at a temperature of 1.1 K) shows that the superconducting energy gap of the substrate is framed by characteristic coherence peaks in an energy range of 2.0−2.7 meV (black d*I*/d*V* spectrum in Figure 1e). The origin of

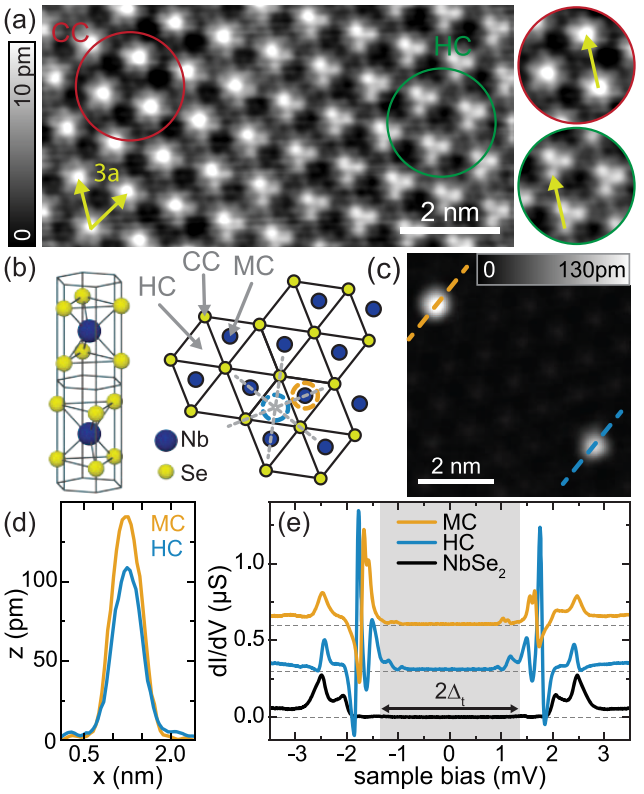

Figure 1. (a) Atomic-resolution STM images showing the incommensurate CDW modulation (constant-current set point: 4 mV, 200 pA) with close-ups of different regions. (b) Unit cell and top view of 2*H*-$NbSe_2$ with different lattice sites labeled as HC, CC, and MC. Gray dashed lines indicate mirror axes. (c) Topography of HC and MC adatoms. (d) Line profiles across the atoms shown in (c). (e) Constant-height d*I*/d*V* spectra taken on the substrate (black) and on the atoms shown in (c) (set point: 4 mV, 200 pA; V_{rms} = 15 μeV, spectra offset by 0.3 μS). $2\Delta_t$ is indicated by the shaded area.

this peculiar quasiparticle density of states (DOS) has been discussed in terms of multiband or anisotropic superconductivity.[1−9] Notice that we use superconducting Pb tips to improve the energy resolution beyond the Fermi−Dirac limit. The convolution of the DOS of tip and substrate shifts all spectral features by the tip's energy gap $\Delta_t \approx 1.35$ meV (for details see Supporting Information (SI)[48]).

Scanning tunneling microscopy (STM) images of the clean surface clearly reveal the modulation of the local DOS induced by the CDW superimposed on the atomic corrugation (Figure 1a). The CDW has a lattice constant $a_{cdw} \gtrsim 3a$, making it incommensurate with the underlying atomic lattice. Thus, the

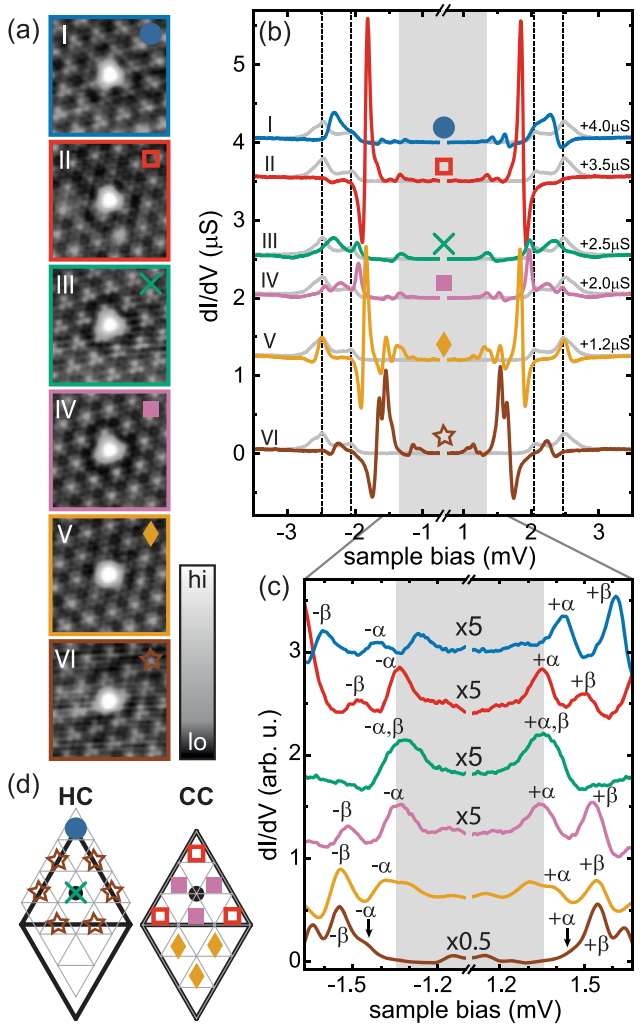

Figure 2. (a) Constant-current STM images (5 × 5 nm^2) of several HC Fe atoms labeled by I−VI. A nonlinear color code is used to resolve the atomic background (set point: 4 mV, 200 pA). (b) Constant-height d*I*/d*V* spectra taken at the center of atoms I−VI (color) and on the substrate (gray). Spectra offset for clarity (set point: 4 mV, 200 pA; V_{rms} = 15 μeV). (c) Close-ups of the spectra in (b). YSR resonances are labeled by $\pm\alpha$, $\pm\beta$. (d) Superimposed atomic (gray) and CDW lattices (black) for two CDW structures (HC and CC). The Se atoms are located at vertices of the atomic grids, so that the HC (MC) adsorption sites correspond to triangles pointing up (down). In the CDW lattice, vertices (dots) are maxima (minima) of the CDW. Colored symbols indicate the positions of atoms I−VI.

phase of the CDW relative to the atomic lattice varies smoothly across the surface.[49,50] The close-ups show two extremal cases for which the maxima coincide either with a Se atom (chalcogen-centered, CC, red circle in Figure 1a) or a hollow site (hollow-centered, HC, green circle in Figure 1a[51]).

Fe atoms (deposited at temperatures below 12 K into the STM) appear as two stable species with different apparent heights (Figure 1c,d). By atomic-resolution imaging (for details see SI[48]), we assign adatoms with small and large apparent height to adsorption in the two inequivalent hollow sites of the terminating Se layer, identified as hollow-centered (HC) and metal-centered (MC) sites, respectively (Figure 1b).[52] d*I*/d*V* spectra taken above the centers of HC and MC adatoms (blue and orange in Figure 1e) show several YSR states inside the superconducting gap as well as in the energy

DOI: 10.1021/acs.nanolett.9b03988
Nano Lett. 2020, 20, 339−344

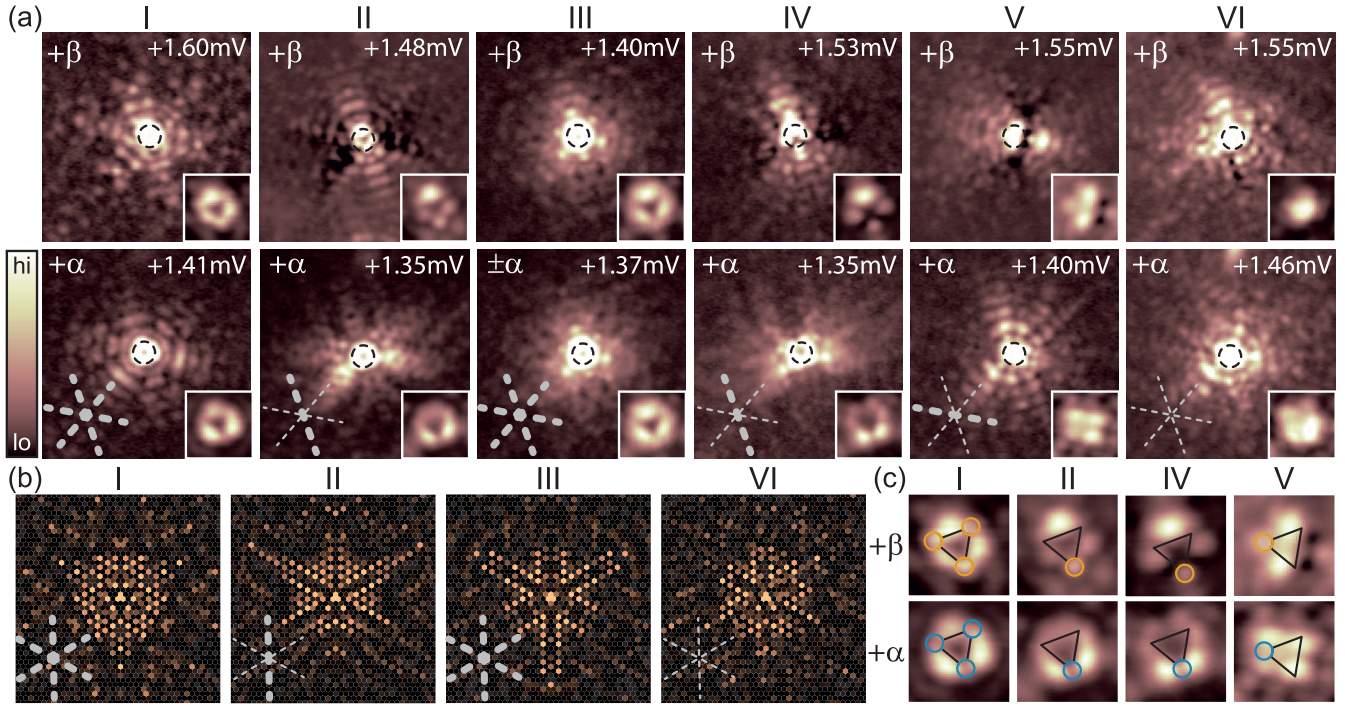

Figure 3. (a) Constant-contour dI/dV maps (9.5 × 9.5 nm^2) of the YSR (α,β) states of HC atoms (I−VI) (set point: 4 mV, 200 pA; V_{rms} = 15−25 μeV; V_{bias} as indicated). Black dashed circles (diameter 1 nm) outline the atoms' position. The insets show a 2 × 2 nm^2 close-up view around the center of the atoms. (b) Numerical results for YSR states within a phenomenological description of the CDW (field of view: 40a × 40a around adatom). For details of the model and parameters, see SI,[48] specifically Figure S2 where these plots are complemented by additional adsorption sites. Thick (thin) gray lines in the maps indicate presence (absence) of mirror axes. (c) Close-up view around the center of the atoms I, II, IV, and V with superimposed triangles illustrating the presence (orange circles) and absence (blue circles) of intensity at their vertices. On atom III, states α and β overlap; on atom VI there is no symmetry.

range of the substrate's coherence peaks as has been observed previously for buried impurities.[42] The energy and intensity of the YSR states differ between the two species. Presumably, the splitting of the adatom d-levels is sensitive to the different local environments of the adsorption sites, which in turn affects the potential- and exchange-scattering strengths.[45]

To isolate the influence of the CDW, we focus on Fe atoms which are all sitting in the same atomic adsorption site (HC) in the following. Six different atoms (labeled by I−VI) are shown in Figure 2a. The corresponding dI/dV spectra (Figure 2b) reveal that the energy and intensity of their YSR states differ strongly even though their atomic adsorption sites are identical with respect to the unperturbed lattice.

YSR states in the energy range of the superconducting coherence peaks are difficult to disentangle from the background. To avoid this complication, we focus on deep-lying YSR states, specifically the two lowest YSR pairs labeled as $\pm\alpha$ and $\pm\beta$ in the close-up view presented in Figure 2c. dI/dV maps recorded at the corresponding bias voltages V_α and V_β are shown in Figure 3a for adatoms I−VI. The main panels show the extended patterns whereas the insets focus on the immediate vicinity of the adatom. All extended maps show patterns with oscillating intensity.[53] The overall symmetries of the patterns clearly differ between adatoms I−VI.

The symmetry of the patterns associated with YSR states is expected to originate from the anisotropy of the Fermi surface[54,55] and the local crystal field.[45] The 3-fold-symmetric atomic adsorption site together with the 6-fold symmetry of the Fermi surface should therefore lead to D_3 symmetry (3-fold rotation as well as three mirror axes, cf. dashed lines in Figure 1b). Interestingly, this D_3 symmetry is observed for both YSR states α and β of adatoms I and III, which reside at a maximum and a minimum of the CDW, respectively (Figures 2d and 3a). However, this symmetry is lost in both, the long-range and the immediate vicinity of the adatoms for the other atoms shown in Figure 3a. For adatoms II, IV, and V, the symmetry is reduced to D_1 symmetry (single mirror axis) whereas no symmetry axis can be discerned for adatom VI.

The symmetry reductions of the YSR patterns coincide with the reductions of the local symmetry of the adsorption sites by the CDW (Figure 2d). Adatoms I and III are positioned at a maximum or a minimum of the CDW, so that the CDW respects the atomic D_3 symmetry (HC structure of the CDW). Atoms II, IV, and V are located on one of the three equivalent symmetry axes connecting the high-symmetry positions but unlike adatoms I and III do not directly fall on an extremum (CDW in the CC domain). Thus, the CDW breaks the atomic D_3 symmetry, leaving only D_1 symmetry consistent with the observed YSR patterns. Finally, the position of adatom VI is totally asymmetric with respect to the CDW, which is reflected in the absence of any symmetry in the corresponding dI/dV maps.

The microscopic physics behind these symmetry reductions can be understood theoretically within a phenomenological mean-field description of the CDW combined with a tight-binding model of the 2H-$NbSe_2$ band structure. Foregoing a realistic description of the Fe d-orbital physics, we model the adatom as a classical impurity with isotropic potential and exchange couplings to the substrate (see SI[48] for details). Because of the electron−phonon interaction, the CDW acts on

DOI: 10.1021/acs.nanolett.9b03988
Nano Lett. 2020, 20, 339−344

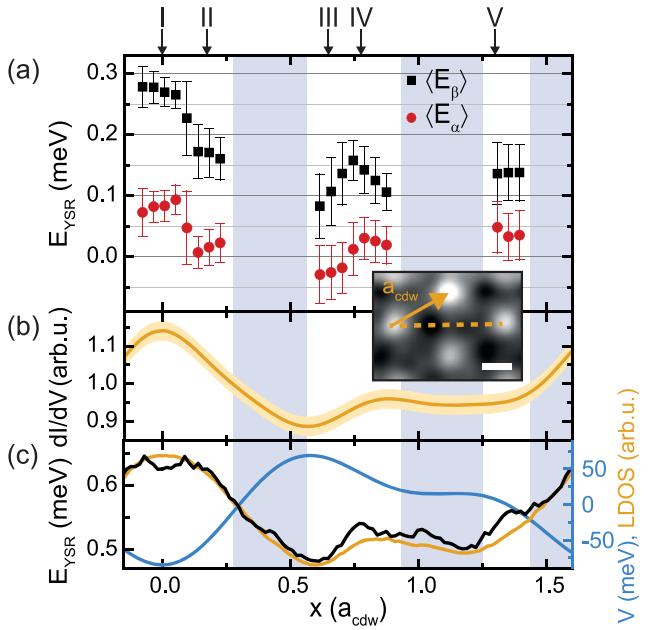

Figure 4. (a) Evolution of the α-, β-YSR energy with position relative to the CDW. Displayed points are obtained from averaging the energies of various atoms within intervals of $x \pm 0.05$ a_{cdw}. Error bars include standard deviation from the averaging method and experimental errors (see SI[48]). (b) Linecut along the orange-dashed line through a FFT-filtered constant-height dI/dV map [taken at T = 8 K and V_{bias} = 0 (set point: 4 mV, 200 pA; V_{rms} = 100 μeV)] shown as the inset (scale bar is 4 Å) representing the variation of the local DOS (the nonfiltered data can be found in Figure S17a). (c) CDW potential (blue), local DOS (orange), and YSR energies (black) obtained from the theoretical model for $JS/2$ = 360 meV, that is, in the strong-coupling regime.

the electrons as a weakly incommensurate, static periodic potential. This potential reduces the symmetry of the YSR wave functions in a manner consistent with the experimental results. Corresponding numerical results are shown in Figure 3b for a subset of the adsorption sites investigated experimentally (see SI[48] for the remaining sites and further details). We find that the wave functions (and the number) of the YSR states are quite sensitive to details of the band structure and the neglected d-orbital physics, so that one expects agreement only for qualitative aspects of symmetry.

So far, the assignments α and β for the YSR states simply refer to the two deepest resonances. Analyzing the observed YSR patterns allows us to track these two YSR states as a function of position relative to the CDW. For the YSR state $+\beta$ of adatom I, the short-range pattern exhibits a triangular shape (Figure 3c) with high intensity on its sides and slightly smaller intensity at its vertices (orange circles). In contrast, the YSR state $+\alpha$ for adatom I lacks intensity at the vertices (blue circles) and thus exhibits pronounced nodes. Signatures of this distinction persist at the lower-symmetry positions II, IV, and V. Although the intensity distributions change for both states, we still observe distinct intensities at one of the vertices which distinguish between the $+\alpha$ and $+\beta$ resonances (while present, the distinction is somewhat less pronounced for adatom V, see also SI[48]). A similar distinction cannot be made for adatom III. We attribute this to the fact that in this case, both the $\pm\alpha$ and the $\pm\beta$ resonances lie very close to the Fermi level. This prevents us from individually resolving them within our energy resolution (Figure 2c, green trace).

With these characteristics, we can track the resonances as a function of position relative to the CDW and probe its effect on the YSR energies. As the CDW transforms smoothly between HC and CC domains, we can study numerous positions along its symmetry axis (such as positions II, IV, and V in Figure 2d but also in between). Altogether, we analyze approximately 90 adatoms adsorbed close to one of the three equivalent CDW symmetry axes, combining data from several samples and Pb tips. For all adatoms, we extract the energies of the YSR states by deconvolving the dI/dV spectra to remove the influence of the Pb tip (see SI[48]). Figure 4a plots the energies of both the α- and β-states as a function of adatom position along a high-symmetry axis of the CDW. Here, we assume that the energy dependences of both resonances follow the same trend which implies that the energy of the α-resonance changes sign and crosses the quantum phase transition from a screened-spin to a free-spin ground state[46,56−58] as a function of adatom position. Note that some regions (shaded in Figure 4a) of adatom positions remain inaccessible for Fe atoms in HC sites, because the CDW maxima avoid MC domains.[51]

A qualitatively similar dependence of the energy of the YSR states is found in our model calculations (Figure 4c and SI[48]). The YSR energies are (anti)correlated with the CDW potential and the local DOS, with the type of correlation depending on whether the impurity is in the weak- or strong-coupling regime and on the strength of potential scattering by the impurity.[48] (We find that the CDW potential is anticorrelated with the local DOS.) Except for very strong potential scattering (see SI[48]), our results are consistent with a simple model for the energy of YSR states[32−34]

$$E_{YSR} = \pm\Delta \frac{1 - \left(\frac{\pi J S \nu_0}{2}\right)^2}{1 + \left(\frac{\pi J S \nu_0}{2}\right)^2} \quad (1)$$

Here, Δ is the superconducting gap, S is the (classical) spin, J is the exchange coupling, and ν_0 is the local DOS of the superconductor. This predicts that YSR energies are (anti)-correlated with the local DOS for impurities in the strong (weak) coupling limit. Experimentally, we record a constant-height dI/dV map at zero bias above T_c and remove the atomic corrugation by an FFT filter (cf. inset Figure 4b). The remaining signal is proportional to the local DOS due to the CDW at the Fermi level. We find that the YSR energies correlate with the local DOS as seen in Figure 4a,b. This suggests that for most adsorption sites, the YSR states are in the strong-coupling regime. Only when the Fe atoms are located in the minima of the CDW, resonance α undergoes the quantum phase transition to the free-spin ground state.

In conclusion, we find that the properties of YSR states are strongly affected by CDW ordering. The CDW shifts the energy of YSR states and reduces the symmetry of YSR wave functions both in the immediate vicinity of and further from the adatoms. These observations impose stringent constraints on the design of strongly coupled magnetic adatom structures on $NbSe_2$ substrates. Nevertheless, $NbSe_2$ remains a highly attractive substrate in this context, owing to the long-range nature of the YSR states and its suitability for adatom manipulation. Our results extend to truly two-dimensional $NbSe_2$ substrates with their promise of device applications. Indeed, single-layer $NbSe_2$ also exhibits an incommensurate CDW.[11,50] Importantly, pairing correlations in single-layer

DOI: 10.1021/acs.nanolett.9b03988
Nano Lett. 2020, 20, 339−344

$NbSe_2$ are remarkably robust against in-plane fields as a consequence of spin-valley locking (Ising superconductivity).[10] This may enable measurements of YSR states at magnetic fields which polarize the adatom spin without suppressing superconductivity. The interaction of YSR states with superconductivity, charge-density order, and external magnetic fields entails substantial flexibility to tune into or control a topologically nontrivial superconducting phase. Finally, our study suggests that YSR states provide a sensitive probe of these competing interactions which should extend to other systems.

■ ASSOCIATED CONTENT

Supporting Information

The Supporting Information is available free of charge at https://pubs.acs.org/doi/10.1021/acs.nanolett.9b03988.

More details of the theoretical considerations (mean-field description of the CDW, tight-binding model, coupling to the magnetic impurity, coupling to the CDW, numerical results) and additional experimental details (superconducting tip, numerical deconvolution of the spectra, identification of adsorption sites, determination of Fe atom position relative to CDW, additional spectra and maps) (PDF)

■ AUTHOR INFORMATION

Corresponding Author

*E-mail: franke@physik.fu-berlin.de.

ORCID

Gaël Reecht: 0000-0001-5036-7271
Benjamin W. Heinrich: 0000-0002-1989-6981
Kai Rossnagel: 0000-0001-5107-0090
Katharina J. Franke: 0000-0001-9416-023X

Notes

The authors declare no competing financial interest.

■ ACKNOWLEDGMENTS

Financial support by Deutsche Forschungsgemeinschaft through Grant CRC 183 (F.v.O.), as well as by the European Research Council through the consolidator grant "NanoSpin" (K.J.F.) is gratefully acknowledged.

■ REFERENCES

(1) Hess, H. F.; Robinson, R. B.; Waszczak, J. V. Vortex-core structure observed with a scanning tunneling microscope. *Phys. Rev. Lett.* **1990**, *64*, 2711−2714.

(2) Yokoya, T.; Kiss, T.; Chainani, A.; Shin, S.; Nohara, M.; Takagi, H. Fermi Surface Sheet-Dependent Superconductivity in 2*H*-$NbSe_2$. *Science* **2001**, *294*, 2518−2520.

(3) Noat, Y.; Cren, T.; Debontridder, F.; Roditchev, D.; Sacks, W.; Toulemonde, P.; San Miguel, A. Signatures of multigap superconductivity in tunneling spectroscopy. *Phys. Rev. B: Condens. Matter Mater. Phys.* **2010**, *82*, 014531.

(4) Noat, Y.; Silva-Guillén, J. A.; Cren, T.; Cherkez, V.; Brun, C.; Pons, S.; Debontridder, F.; Roditchev, D.; Sacks, W.; Cario, L.; Ordejón, P.; García, A.; Canadell, E. Quasiparticle spectra of 2*H* − $NbSe_2$: Two-band superconductivity and the role of tunneling selectivity. *Phys. Rev. B: Condens. Matter Mater. Phys.* **2015**, *92*, 134510.

(5) Rodrigo, J. G.; Vieira, S. STM study of multiband superconductivity in $NbSe_2$ using a superconducting tip. *Phys. C* **2004**, *404*, 306−310.

(6) Boaknin, E.; Tanatar, M. A.; Paglione, J.; Hawthorn, D.; Ronning, F.; Hill, R. W.; Sutherland, M.; Taillefer, L.; Sonier, J.; Hayden, S. M.; Brill, J. W. Heat Conduction in the Vortex State of $NbSe_2$: Evidence for Multiband Superconductivity. *Phys. Rev. Lett.* **2003**, *90*, 117003.

(7) Fletcher, J. D.; Carrington, A.; Diener, P.; Rodière, P.; Brison, J. P.; Prozorov, R.; Olheiser, T.; Giannetta, R. W. Penetration Depth Study of Superconducting Gap Structure of 2*H* − $NbSe_2$. *Phys. Rev. Lett.* **2007**, *98*, 057003.

(8) Guillamón, I.; Suderow, H.; Guinea, F.; Vieira, S. Intrinsic atomic-scale modulations of the superconducting gap of 2*H* − $NbSe_2$. *Phys. Rev. B: Condens. Matter Mater. Phys.* **2008**, *77*, 134505.

(9) Guillamón, I.; Suderow, H.; Vieira, S.; Cario, L.; Diener, P.; Rodière, P. Superconducting Density of States and Vortex Cores of 2H-NbS_2. *Phys. Rev. Lett.* **2008**, *101*, 166407.

(10) Xi, X.; Wang, Z.; Zhao, W.; Park, J.-H.; Law, K. T.; Berger, H.; Forró, L.; Shan, J.; Mak, K. F. Ising pairing in superconducting $NbSe_2$ atomic layers. *Nat. Phys.* **2016**, *12*, 139−143.

(11) Ugeda, M. M.; Bradley, A. J.; Zhang, Y.; Onishi, S.; Chen, Y.; Ruan, W.; Ojeda-Aristizabal, C.; Ryu, H.; Edmonds, M. T.; Tsai, H.-Z.; et al. Characterization of collective ground states in single-layer $NbSe_2$. *Nat. Phys.* **2016**, *12*, 92−97.

(12) Rossnagel, K.; Seifarth, O.; Kipp, L.; Skibowski, M.; Voß, D.; Krüger, P.; Mazur, A.; Pollmann, J. Fermi surface of 2*H* − $NbSe_2$ and its implications on the charge-density-wave mechanism. *Phys. Rev. B: Condens. Matter Mater. Phys.* **2001**, *64*, 235119.

(13) Johannes, M. D.; Mazin, I. I.; Howells, C. A. Fermi-surface nesting and the origin of the charge-density wave in $NbSe_2$. *Phys. Rev. B: Condens. Matter Mater. Phys.* **2006**, *73*, 205102.

(14) Kiss, T.; Yokoya, T.; Chainani, A.; Shin, S.; Hanaguri, T.; Nohara, M.; Takagi, H. Charge-order-maximized momentum-dependent superconductivity. *Nat. Phys.* **2007**, *3*, 720−725.

(15) Johannes, M. D.; Mazin, I. I. Fermi surface nesting and the origin of charge density waves in metals. *Phys. Rev. B: Condens. Matter Mater. Phys.* **2008**, *77*, 165135.

(16) Rahn, D. J.; Hellmann, S.; Kalläne, M.; Sohrt, C.; Kim, T. K.; Kipp, L.; Rossnagel, K. Gaps and kinks in the electronic structure of the superconductor 2*H*-$NbSe_2$ from angle-resolved photoemission at 1 K. *Phys. Rev. B: Condens. Matter Mater. Phys.* **2012**, *85*, 224532.

(17) Malliakas, C. D.; Kanatzidis, M. G. Nb-Nb Interactions Define the Charge Density Wave Structure of 2H-$NbSe_2$. *J. Am. Chem. Soc.* **2013**, *135*, 1719−22.

(18) Dai, J.; Calleja, E.; Alldredge, J.; Zhu, X.; Li, L.; Lu, W.; Sun, Y.; Wolf, T.; Berger, H.; McElroy, K. Microscopic evidence for strong periodic lattice distortion in two-dimensional charge-density wave systems. *Phys. Rev. B: Condens. Matter Mater. Phys.* **2014**, *89*, 165140.

(19) Arguello, C. J.; Chockalingam, S. P.; Rosenthal, E. P.; Zhao, L.; Gutiérrez, C.; Kang, J. H.; Chung, W. C.; Fernandes, R. M.; Jia, S.; Millis, A. J.; Cava, R. J.; Pasupathy, A. N. Visualizing the charge density wave transition in 2*H*-$NbSe_2$ in real space. *Phys. Rev. B: Condens. Matter Mater. Phys.* **2014**, *89*, 235115.

(20) Arguello, C. J.; Rosenthal, E. P.; Andrade, E. F.; Jin, W.; Yeh, P. C.; Zaki, N.; Jia, S.; Cava, R. J.; Fernandes, R. M.; Millis, A. J.; Valla, T.; Osgood, R. M.; Pasupathy, A. N. Quasiparticle Interference, Quasiparticle Interactions, and the Origin of the Charge Density Wave in 2*H* − $NbSe_2$. *Phys. Rev. Lett.* **2015**, *114*, 037001.

(21) Flicker, F.; van Wezel, J. Charge order from orbital-dependent coupling evidenced by $NbSe_2$. *Nat. Commun.* **2015**, *6*, 7034.

(22) Soumyanarayanan, A.; Yee, M. M.; He, Y.; van Wezel, J.; Rahn, D. J.; Rossnagel, K.; Hudson, E. W.; Norman, M. R.; Hoffman, J. E. Quantum phase transition from triangular to stripe charge order in $NbSe_2$. *Proc. Natl. Acad. Sci. U. S. A.* **2013**, *110*, 1623−7.

(23) Weber, F.; Rosenkranz, S.; Castellan, J.-P.; Osborn, R.; Hott, R.; Heid, R.; Bohnen, K.-P.; Egami, T.; Said, A. H.; Reznik, D. Extended Phonon Collapse and the Origin of the Charge-Density Wave in 2*H* − $NbSe_2$. *Phys. Rev. Lett.* **2011**, *107*, 107403.

(24) Suderow, H.; Tissen, V. G.; Brison, J. P.; Martínez, J. L.; Vieira, S. Pressure Induced Effects on the Fermi Surface of Superconducting 2H − $NbSe_2$. *Phys. Rev. Lett.* **2005**, *95*, 117006.

DOI: 10.1021/acs.nanolett.9b03988
Nano Lett. 2020, 20, 339−344

(25) Borisenko, S. V.; Kordyuk, A. A.; Zabolotnyy, V. B.; Inosov, D. S.; Evtushinsky, D.; Büchner, B.; Yaresko, A. N.; Varykhalov, A.; Follath, R.; Eberhardt, W.; Patthey, L.; Berger, H. Two Energy Gaps and Fermi-Surface "Arcs" in $NbSe_2$. *Phys. Rev. Lett.* **2009**, *102*, 166402.
(26) Cho, K.; Konczykowski, M.; Teknowijoyo, S.; Tanatar, M. A.; Guss, J.; Gartin, P. B.; Wilde, J. M.; Kreyssig, A.; McQueeney, R. J.; Goldman, A. I.; Mishra, V.; Hirschfeld, P. J.; Prozorov, R.; et al. Using controlled disorder to probe the interplay between charge order and superconductivity in $NbSe_2$. *Nat. Commun.* **2018**, *9*, 2796.
(27) Sticlet, D.; Morari, C. Topological superconductivity from magnetic impurities on monolayer $NbSe_2$. *Phys. Rev. B: Condens. Matter Mater. Phys.* **2019**, *100*, 075420.
(28) Głodzik, S.; Ojanen, T. Engineering nodal topological phases in Ising superconductors by magnetic superstructures. 2019 arXiv1905.01063v1.
(29) Nadj-Perge, S.; Drozdov, I. K.; Li, J.; Chen, H.; Jeon, S.; Seo, J.; MacDonald, A. H.; Bernevig, B. A.; Yazdani, A. Observation of Majorana fermions in ferromagnetic atomic chains on a superconductor. *Science* **2014**, *346*, 602−607.
(30) Nadj-Perge, S.; Drozdov, I. K.; Bernevig, B. A.; Yazdani, A. Proposal for realizing Majorana fermions in chains of magnetic atoms on a superconductor. *Phys. Rev. B: Condens. Matter Mater. Phys.* **2013**, *88*, 020407.
(31) Pientka, F.; Glazman, L. I.; von Oppen, F. Topological superconducting phase in helical Shiba chains. *Phys. Rev. B: Condens. Matter Mater. Phys.* **2013**, *88*, 155420.
(32) Yu, L. Bound State in Superconductors With Paramagnetic Impurities. *Acta Phys. Sin.* **1965**, *21*, 75−91.
(33) Shiba, H. Classical Spins in Superconductors. *Prog. Theor. Phys.* **1968**, *40*, 435−451.
(34) Rusinov, A. I. Superconcductivity near a Paramagnetic Impurity. *JETP Lett.* **1969**, *9*, 85.
(35) Yazdani, A.; Jones, B. A.; Lutz, C. P.; Crommie, M. F.; Eigler, D. M. Probing the Local Effects of Magnetic Impurities on Superconductivity. *Science* **1997**, *275*, 1767−1770.
(36) Ménard, G. C.; Guissart, S.; Brun, C.; Pons, S.; Stolyarov, V. S.; Debontridder, F.; Leclerc, M. V.; Janod, E.; Cario, L.; Roditchev, D.; Simon, P.; Cren, T. Coherent long-range magnetic bound states in a superconductor. *Nat. Phys.* **2015**, *11*, 1013.
(37) Kezilebieke, S.; Dvorak, M.; Ojanen, T.; Liljeroth, P. Coupled Yu-Shiba-Rusinov States in Molecular Dimers on $NbSe_2$. *Nano Lett.* **2018**, *18*, 2311−2315.
(38) Ruby, M.; Heinrich, B. W.; Peng, Y.; von Oppen, F.; Franke, K. J. Wave-Function Hybridization in Yu-Shiba-Rusinov Dimers. *Phys. Rev. Lett.* **2018**, *120*, 156803.
(39) Choi, D.-J.; Fernández, C. G.; Herrera, E.; Rubio-Verdú, C.; Ugeda, M. M.; Guillamón, I.; Suderow, H.; Pascual, J. I.; Lorente, N. Influence of Magnetic Ordering between Cr Adatoms on the Yu-Shiba-Rusinov States of the $\beta - Bi_2Pd$ Superconductor. *Phys. Rev. Lett.* **2018**, *120*, 167001.
(40) Kamlapure, A.; Cornils, L.; Wiebe, J.; Wiesendanger, R. Engineering the spin couplings in atomically crafted spin chains on an elemental superconductor. *Nat. Commun.* **2018**, *9*, 1−7.
(41) Kim, H.; Palacio-Morales, A.; Posske, T.; Rózsa, L.; Palotás, K.; Szunyogh, L.; Thorwart, M.; Wiesendanger, R. Toward tailoring Majorana bound states in artificially constructed magnetic atom chains on elemental superconductors. *Science Advances* **2018**, *4*, No. eaar5251.
(42) Senkpiel, J.; Rubio-Verdú, C.; Etzkorn, M.; Drost, R.; Schoop, L. M.; Dambach, S.; Padurariu, C.; Kubala, B.; Ankerhold, J.; Ast, C. R.; Kern, K. Robustness of Yu-Shiba-Rusinov resonances in the presence of a complex superconducting order parameter. *Phys. Rev. B: Condens. Matter Mater. Phys.* **2019**, *100*, 014502.
(43) Ji, S.-H.; Zhang, T.; Fu, Y.-S.; Chen, X.; Ma, X.-C.; Li, J.; Duan, W.-H.; Jia, J.-F.; Xue, Q.-K. High-Resolution Scanning Tunneling Spectroscopy of Magnetic Impurity Induced Bound States in the Superconducting Gap of Pb Thin Films. *Phys. Rev. Lett.* **2008**, *100*, 226801.
(44) Ruby, M.; Pientka, F.; Peng, Y.; von Oppen, F.; Heinrich, B. W.; Franke, K. J. Tunneling Processes into Localized Subgap States in Superconductors. *Phys. Rev. Lett.* **2015**, *115*, 087001.
(45) Ruby, M.; Peng, Y.; von Oppen, F.; Heinrich, B. W.; Franke, K. J. Orbital Picture of Yu-Shiba-Rusinov Multiplets. *Phys. Rev. Lett.* **2016**, *117*, 186801.
(46) Choi, D.-J.; Rubio-Verdú, C.; De Bruijckere, J.; Ugeda, M. M.; Lorente, N.; Pascual, J. I. Mapping the orbital structure of impurity bound states in a superconductor. *Nat. Commun.* **2017**, *8*, 15175.
(47) Cornils, L.; Kamlapure, A.; Zhou, L.; Pradhan, S.; Khajetoorians, A. A.; Fransson, J.; Wiebe, J.; Wiesendanger, R. Spin-Resolved Spectroscopy of the Yu-Shiba-Rusinov States of Individual Atoms. *Phys. Rev. Lett.* **2017**, *119*, 197002.
(48) Supporting Information.
(49) Gye, G.; Oh, E.; Yeom, H. W. Topological Landscape of Competing Charge Density Waves in $2H - NbSe_2$. *Phys. Rev. Lett.* **2019**, *122*, 016403.
(50) Guster, B.; Rubio-Verdú, C.; Robles, R.; Zaldívar, J.; Dreher, P.; Pruneda, M.; Silva-Guillén, J. Á.; Choi, D.-J.; Pascual, J. I.; Ugeda, M. M.; Ordejón, P.; Canadell, E. Coexistence of Elastic Modulations in the Charge Density Wave State of $2H$-$NbSe_2$. *Nano Lett.* **2019**, *19*, 3027−3032.
(51) Areas with Nb-centered CDW maxima (metal-centered, MC) do not appear in the STM images, as they have higher energy.[49,50] See SI,[48] especially Figure S18 for further details.
(52) In addition to the apparent height, both species also differ in the energies of their *d*-level resonances. We note that the apparent heights and *d*-level resonances are only slightly affected by the CDW. See SI[48] for more details.
(53) The long-range oscillations are expected to have a period of half the Fermi wavelength in simple models of YSR states.[34] The Fermi surface of $2H$-$NbSe_2$ consists of several sheets[2,12,14,16] which can lead to a more complex structure in the long-range scattering pattern of the YSR wave functions.
(54) Salkola, M. I.; Balatsky, A. V.; Schrieffer, J. R. Spectral properties of quasiparticle excitations induced by magnetic moments in superconductors. *Phys. Rev. B: Condens. Matter Mater. Phys.* **1997**, *55*, 12648−12661.
(55) Flatté, M. E.; Byers, J. M. Local Electronic Structure of a Single Magnetic Impurity in a Superconductor. *Phys. Rev. Lett.* **1997**, *78*, 3761−3764.
(56) Franke, K. J.; Schulze, G.; Pascual, J. I. Competition of Superconducting Phenomena and Kondo Screening at the Nanoscale. *Science* **2011**, *332*, 940−944.
(57) Farinacci, L.; Ahmadi, G.; Reecht, G.; Ruby, M.; Bogdanoff, N.; Peters, O.; Heinrich, B. W.; von Oppen, F.; Franke, K. J. Tuning the Coupling of an Individual Magnetic Impurity to a Superconductor: Quantum Phase Transition and Transport. *Phys. Rev. Lett.* **2018**, *121*, 196803.
(58) Malavolti, L.; Briganti, M.; Hänze, M.; Serrano, G.; Cimatti, I.; McMurtrie, G.; Otero, E.; Ohresser, P.; Totti, F.; Mannini, M.; Sessoli, R.; Loth, S. Tunable Spin-Superconductor Coupling of Spin 1/2 Vanadyl Phthalocyanine Molecules. *Nano Lett.* **2018**, *18*, 7955−7961.

DOI: 10.1021/acs.nanolett.9b03988
Nano Lett. 2020, 20, 339−344